Supplementary information

Hannu-Pekka Komsa, Natalia Berseneva, Arkady V. Krasheninnikov, and Risto M. Nieminen

Department of Applied Physics, Aalto University,

P.O. Box 11100, 00076 Aalto, Finland

(Dated: May 15, 2014)

I. METHOD

Following Ref. 1, the correction is defined as the difference between the electrostatic energy of an isolated charge distribution $\rho(\mathbf{r})$ (the "additional" defect charge) and the same charge experiencing periodic boundary conditions

$$E_{\text{corr}} = E_{\text{isolated}} - E_{\text{periodic}} + q\Delta V, \tag{1}$$

where q is the defect charge (integrated charge of $\rho(\mathbf{r})$) and ΔV is a potential alignment term. The electrostatic energy $E = \frac{1}{2}\int V(\mathbf{r})\rho(\mathbf{r})d\mathbf{r}$, where $V(\mathbf{r})$ is the electrostatic potential emanating from charge $\rho(\mathbf{r})$ and obtained through the solution of the Poisson equation. Since the self-energy is canceled out in the above equation, the correction is not sensitive to the chosen defect charge distribution $\rho(\mathbf{r})$ (except for its second radial moment), and some simple model distribution (e.g. a Gaussian) can thus be adopted. The shift ΔV is determined from the difference of the model potential (obtained from the model charge) and of the electrostatic potential obtained from the electronic-structure calculations far from the defect [2]. It can be shown that the $q\Delta V$ term removes the dependence on the second radial moment of the model charge distribution [2–4].

Poisson equation in the full form is

$$\nabla \cdot (\varepsilon(\mathbf{r})\nabla V(\mathbf{r})) = -\rho(\mathbf{r}) \tag{2}$$

where the permittivity ε is a second-rank tensor depending locally on the position $\mathbf{r}$. We note that ε is a required input for the correction scheme. It reduces to a simple constant (homogeneous throughout the system) in many bulk systems, but becomes more complicated in the low-dimensional systems. We limit our study to systems for which the permittivity depends only on z. Also, in our case the lateral and perpendicular components may differ,

but it is sufficient to consider only the diagonal components: $\left(\varepsilon_{\parallel}, \varepsilon_{\parallel}, \varepsilon_{\perp}\right)$. The Poisson equation may then be written as:

$$\varepsilon_{\parallel}(z)\frac{\partial^2}{\partial x^2}V(r) + \varepsilon_{\parallel}(z)\frac{\partial^2}{\partial y^2}V(r) + \varepsilon_{\perp}(z)\frac{\partial^2}{\partial z^2}V(r) + \frac{\partial}{\partial z}\varepsilon_{\perp}(z)\frac{\partial}{\partial z}V(r) = -\rho(r). \tag{3}$$

This is solved under periodic boundary conditions in Fourier space [1]. The average potential over the supercell is set to zero in correspondence with the convention adopted in electronic structure calculations, thereby automatically leading to the inclusion of homogeneous neutralizing background charge.

Finally, the energy of isolated defect E_{isolated} is obtained through extrapolation of E_{periodic} by uniformly scaling in all directions (with a scaling factor α) the supercell size to the limit of infinitely large supercell. Simple polynomial fits of the form $a + b\alpha^{-1} + c\alpha^{-2} \ldots$ worked well in our case.

To summarize, the correction involves the following steps:

1. Construct dielectric constant profile $\varepsilon(z)$. Here, the profile is taken to follow the charge density distribution of the host, but with yet unknown normalization within the material. The dielectric constants over the whole supercell are calculated using density functional perturbation theory. Finally, the profile is normalized such that the conditions in Eqs. (2) and (3) in the main paper are satisfied.

2. Choose model charge distribution $\rho(\mathbf{r})$. Here taken as a simple Gaussian to the first approximation.

3. Solve model potential V subject to periodic boundary conditions using $\rho(\mathbf{r})$ and $\varepsilon(z)$.

4. Calculate E_{periodic}.

5. Obtain E_{isolated} from E_{periodic} by uniformly scaling the supercell size.

6. Compare model potential to DFT potential to get ΔV

Thus, all terms of Eq. 1 are now known and E_{corr} may be determined.

II. MODEL PARAMETERS

For BN, the macroscopic dielectric constant profile is constructed using a Gaussian with standard deviation $\sigma = 1.48$ bohr, in agreement with the fit to the valence electron density

distribution from the DFT calculation. The profiles are shown under Model #1 in Fig. 2. Due to the form of condition in Eq. 3 of the main paper, which has integral over inverses, as the profile width is decreased, the local dielectric constant has to be changed more strongly than with Eq. 2 in order for the integral to remain at the desired value. That is, the local inverse dielectric constant (or inverse polarizability) within the slab can get close to zero and consequently the dielectric constant becomes large. With a Gaussian model charge the corrected formation energies were somewhat overestimated. We thus modified the model in accordance with the charge density difference obtained from DFT (charged defect density minus the bulk density), as shown in Fig. 1, yielding flat corrected formation energies. We note that, even with the simple Gaussian model the extrapolated energies agree. Finally, as shown in Fig. 2, the electrostatic potentials from the DFT (charged defect minus the bulk) and from the model agree reasonably well throughout the cell apart from the close vicinity of the defect.

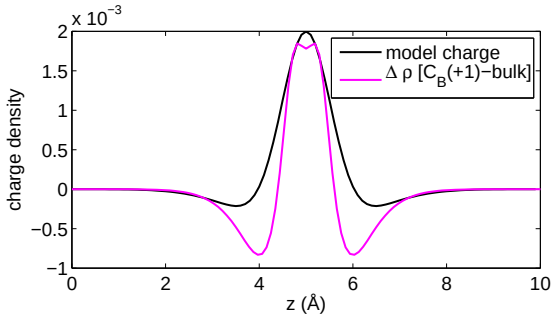

FIG. 1. Model charge density and density difference from DFT (charged defect density minus the bulk density).

We show in Fig. 2 results for three other dielectric constant profile models. It can be seen, that changing the width or the shape of the profile has relatively minor effect on the corrected energies. On the othed hand, if the profiles are not normalized according to Eqs. (2) and (3) of the main text, the corrections deviate much more. Still, in all cases, the extrapolated values agree.

For MoS_2, edges are located at 4.4 Å from the center of the layer, smoothness of the error function edges is 1.0 bohr. The charge models for the $Mn_{Mo}(+1)$ and $F_S(+1)$ are shown in Fig. 5(a), and show similar compensation charge near the interface as for the BN defects. The corresponding electrostatic potentials in the case of $F_S(+1)$ are shown in Fig. 5(b).

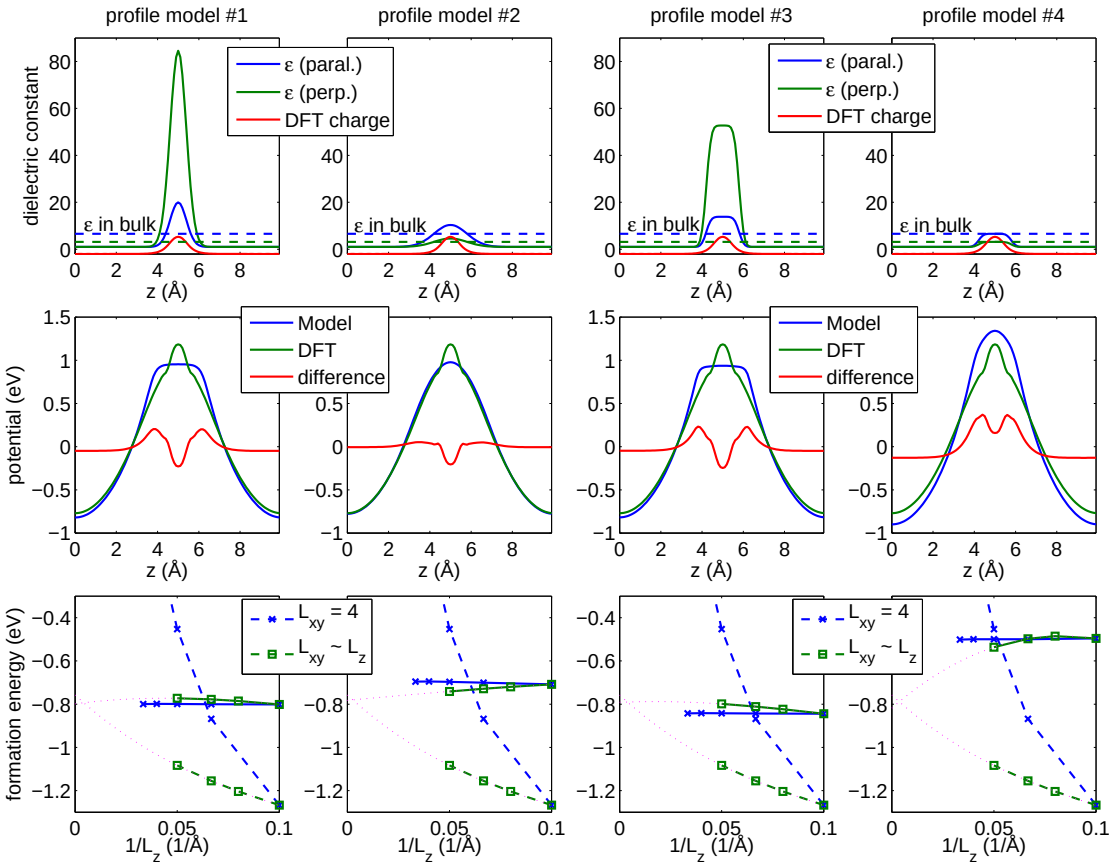

FIG. 2. Application of the correction for $C_B(+1)$ defect in BN with four different dielectric constant profiles. Model #1: The model suggested in the main text. Model #2: Same as #1 but with lateral Gaussian width $\sigma = 3$ bohr. Model #3: Square profile with thickness of 3 bohr and edge smoothness 0.5 bohr. Model #4: Same as #3 but without enforcing the normalization conditions given in Eqs. 2 and 3 in the main text. First row: Model dielectric constant profile and comparison to plane-averaged charge density from DFT. The macroscopic dielectric constants of bulk $h-$BN are also shown as horizontal dashed lines. Second row: Electrostatic potentials from the model and from DFT, along with their difference. Third row: Defect formation energies for the 4×4 and uniformly scaled systems. The fits used for extrapolation use powers of L^{-1} up to third order.

In the case of BN, the ΔV values obtained from the difference between the model and DFT potentials were very close to zero, but they differ by several tens of meVs in the case of MoS_2. This could possibly be fixed by tuning the dielectric constant profile or the charge model. On the other hand, the obtained ΔV values depend quite linearly on the volume

(as they should). This allowed us to include their contribution to the energy correction by simply extracting the corresponding linear coefficient.

III. ADDITIONAL RESULTS

A. *h*-BN

Here we report results for a few additional defects. Fig. 3 shows the results for 4 carbon atom substituting 3 N and 1 B or 1 B and 3 N. These were considered in Refs. [5, 6]. The stable charge states for these are +1 and +2 for the former, and −1 and −2 for the latter.

There is a dramatic deviation from a straight line for 4×4 supercell with large vacuum. In the case of negatively charged defects, the neutralizing background charge is positive, which leads to positive curvature of the electrostatic potential in the vacuum and subsequently the potential is pushed low in the middle of the vacuum region. As demonstrated in Fig. 4, with increasing size of the vacuum region, the potential dips lower and lower and finally electronic charge density starts building up in the middle of the vacuum. It is at this point that the defect formation energies start to deviate strongly from the correct energy. Such spurious energy contributions are not accounted for in the correction, but at least their presence is easily observed from the deviation as well as from the comparison of model and DFT potentials. The same electron leakage effect has been observed previously in calculation of layer exfoliation by charging [7].

B. MoS_2

We show in Fig. 5(c,d) the charge transition levels for Mn_{Mo} and F_S defects as a function of the inverse supercell size in z-direction.

[1] H.-P. Komsa and A. Pasquarello, Phys. Rev. Lett. **110**, 095505 (2013).

[2] C. Freysoldt, J. Neugebauer, and C. G. Van de Walle, Phys. Rev. Lett. **102**, 016402 (2009).

[3] I. Dabo, B. Kozinsky, N. E. Singh-Miller, and N. Marzari, Phys. Rev. B **77**, 115139 (2008).

[4] H.-P. Komsa, T. T. Rantala, and A. Pasquarello, Phys. Rev. B **86**, 045112 (2012).

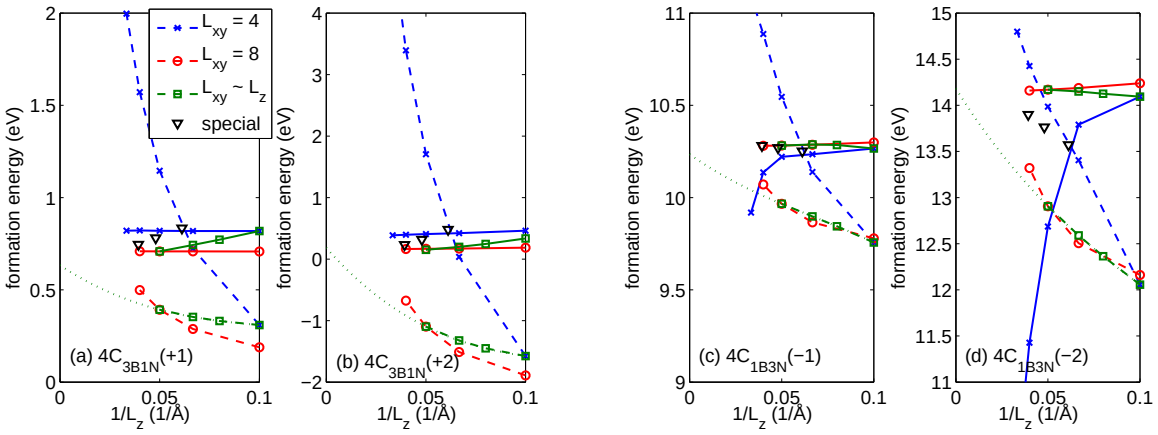

FIG. 3. Defect formation energies for 4 carbon triangular defects in h-BN: (a) $4C_{3B1N}(+1)$ (b) $4C_{3B1N}(+2)$ (c) $4C_{1B3N}(-1)$ (d) $4C_{1B3N}(-2)$. Notation as in Fig. 2(b) of the main paper.

[5] N. Berseneva, A. V. Krasheninnikov, and R. M. Nieminen, Phys. Rev. Lett. **107**, 035501 (2011).

[6] N. Berseneva, A. Gulans, A. V. Krasheninnikov, and R. M. Nieminen, Phys. Rev. B **87**, 035404 (2013).

[7] M. Topsakal and S. Ciraci, Phys. Rev. B **85**, 045121 (2012).

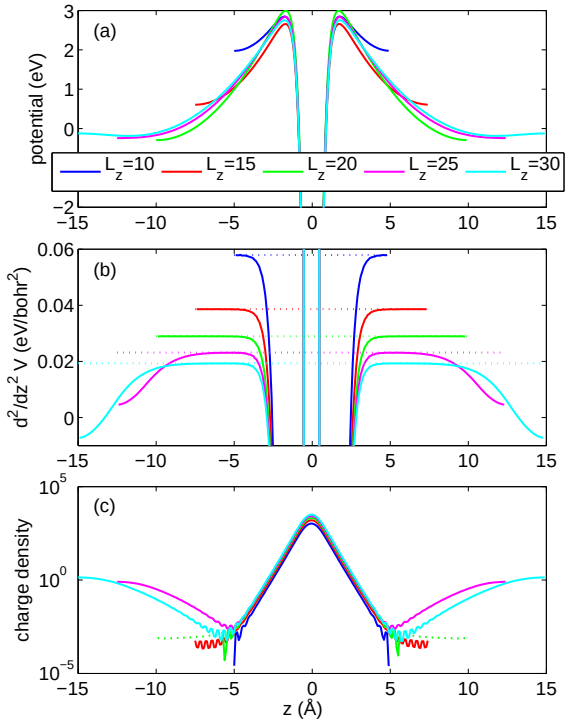

FIG. 4. (a) Planar-averaged electrostatic potential of $4C_{1B3N}$(-1) at varying vacuum size. (b) Second derivative of the potential (solid) and the level of parabolicity obtained from Poisson equation for the neutralizing background charge (dotted) $\frac{\partial^2 V}{\partial z^2} = 4\pi \frac{q}{\Omega}$, where Ω is volume of the supercell. (c) The corresponding valence charge density distributions showing only exponential decay (straight line in the semi-log scale) near the BN layer (at $z = 0$) for vacuums up to 20 Å. For larger vacuums, Gaussian (parabolic in the semi-log scale) charge builds up at the center of the vacuum.

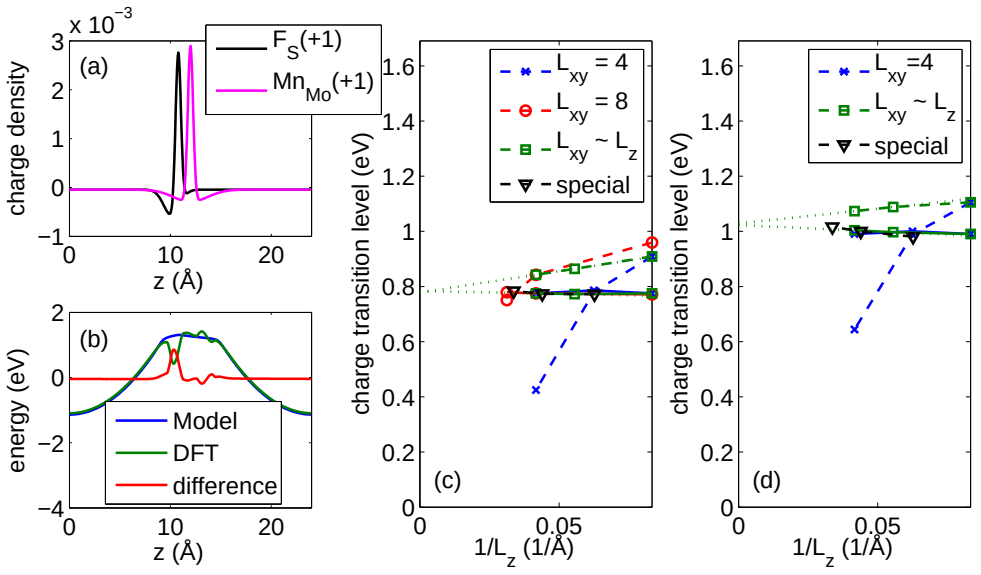

FIG. 5. (a) Model charges for $F_S(+1)$ and for $Mn_{Mo}(+1)$ in MoS_2. (b) Electrostatic potentials from DFT, from the model, and their difference in the case of $F_S(+1)$. (c,d) Charge transition levels $\varepsilon(0/+1)$ as a function of the inverse supercell in z-direction for Mn_{Mo} and F_S defects. The scale of y-axis is limited by the PBE band gap of monolayer MoS_2 (1.69 eV). Notation as in Fig. 1(c) in the main paper.